JOURNAL OF GEOPHYSICAL RESEARCH, VOL. 113, D15S18, doi:10.1029/2007JD008807, 2008

Click Here for Full Article

Global estimates of gravity wave momentum flux from High Resolution Dynamics Limb Sounder observations

M. J. Alexander,[1] J. Gille,[2,3] C. Cavanaugh,[3] M. Coffey,[3] C. Craig,[3] T. Eden,[3] G. Francis,[3] C. Halvorson,[3] J. Hannigan,[3] R. Khosravi,[3] D. Kinnison,[3] H. Lee,[3,4] S. Massie,[3] B. Nardi,[3] J. Barnett,[5] C. Hepplewhite,[5] A. Lambert,[6] and V. Dean[2]

Received 13 April 2007; revised 22 October 2007; accepted 7 December 2007; published 9 May 2008.

[1] High Resolution Dynamics Limb Sounder (HIRDLS) temperature profiles are analyzed to derive global properties of gravity waves. We describe a wavelet analysis technique that determines covarying wave temperature amplitude in adjacent temperature profile pairs, the wave vertical wavelength as a function of height, and the horizontal wave number along the line joining each profile pair. The analysis allows a local estimate of the magnitude of gravity wave momentum flux as a function of geographic location and height on a daily basis. We examine global distributions of these gravity wave properties in the monthly mean and on an individual day, and we also show sample instantaneous wave events observed by HIRDLS. The results are discussed in terms of previous satellite and radiosonde observational analyses and middle atmosphere general circulation model studies that parameterize gravity wave effects on the mean flow. The high vertical and horizontal resolution afforded by the HIRDLS measurements allows the analysis of a wider range of wave vertical and horizontal wavelengths than previous studies and begins to show individual wave events associated with mountains and convection in high detail. Mountain wave observations show clear propagation to altitudes in the mesosphere.

Citation: Alexander, M. J., et al. (2008), Global estimates of gravity wave momentum flux from High Resolution Dynamics Limb Sounder observations, *J. Geophys. Res.*, *113*, D15S18, doi:10.1029/2007JD008807.

1. Introduction

[2] Gravity waves drive large-scale circulations in the atmosphere, and are treated via parameterization in most modern general circulation models. The effects of mountain wave drag are parameterized in most climate models, and the effects of nonstationary waves are important in models seeking a realistic middle atmosphere circulation, including chemistry-climate models that forecast long-term ozone changes. Gravity wave parameterizations require detailed information on global variations in the spectrum of wave vertical flux of horizontal pseudomomentum, hereafter referred to as simply momentum flux. Important known sources for gravity waves include topography, convection, and unbalanced winds. Waves emanating from these sources are known to exhibit both geographical and temporal variations. Satellite observations offer the best hope of quantifying the needed information on a global scale. Progressive advances in satellite-borne instrument resolution and precision have allowed observation of smaller-scale gravity waves and their global properties. Gravity waves are generally detected in satellite observations as temperature fluctuations. The conversion of measured wave temperature amplitude to momentum flux requires simultaneous observation of the vertical and horizontal wavelengths and wave propagation direction. Techniques for estimating momentum flux from space-borne temperature profile data have suffered from large uncertainty, primarily due to the limited horizontal sampling of the measurements [*Eckermann and Preusse*, 1999; *Ern et al.*, 2004, 2006]. Recent advances in horizontal sampling by instruments on the Aqua and Aura satellites not only reduce this uncertainty, but in some cases are now providing a fully resolved three-dimensional view of gravity waves from space [*Wu and Zhang*, 2004; *Eckermann et al.*, 2006; *Alexander and Teitelbaum*, 2007].

[3] Different satellite measurement techniques resolve different portions of the full spectrum of gravity waves that can be present in the atmosphere. For example, the high horizontal resolution Atmospheric Infrared Sounder (AIRS) observations, with a 13.5-km nadir footprint and imaging capability, have deep vertical weighting functions that limit the detection of waves to those with vertical wavelengths longer than 12 km. *Alexander and Barnet* [2007] describe how the measurement weighting functions for different

[1]NWRA, Colorado Research Associates Division, Boulder, Colorado, USA.
[2]Center for Limb Atmospheric Sounding, University of Colorado, Boulder, Colorado, USA.
[3]National Center for Atmospheric Research, Boulder, Colorado, USA.
[4]Deceased July 2007.
[5]Clarendon Laboratory, Oxford University, Oxford, UK.
[6]Jet Propulsion Laboratory, California Institute of Technology, Pasadena, California, USA.

Copyright 2008 by the American Geophysical Union.
0148-0227/08/2007JD008807$09.00

satellite measurement techniques convolve with the three-dimensional gravity wavefield to limit the range of wave types that can be observed. These limitations can sometimes control the patterns in observed temperature variance [*Alexander*, 1998]. *Preusse et al.* [2000] showed that by artificially limiting the analyzed range of vertical wavelengths, CRISTA (Cryogenic Infrared Spectrometers and Telescopes for the Atmosphere) data could be shown to agree with previous analyses of data sets with more limited resolution. In contrast to nadir viewing instruments, limb sounders (like HIRDLS and CRISTA) tend to have higher vertical resolution, but have weighting functions that span ~200 km along the line of sight with peak contribution near the tangent point. They can therefore exclude many short horizontal wavelength waves [*Preusse et al.*, 2002].

[4] The High Resolution Dynamics Limb Sounder (HIRDLS) on the NASA EOS-Aura satellite offers the highest vertical resolution to date from an infrared limb profiling instrument in space. The vertical projection of the field of view (FOV) at the limb is ~1 km [*Gille et al.*, 2008]. Oversampling by a factor of 4–5 gives the potential for vertical resolution <1 km. The horizontal along-track sampling is approximately 1° (75–100 km) along the measurement track, but is nominally 24.72° longitude near the equator. The longitudinal sampling is much higher near the turn-around latitudes of the HIRDLS measurement track which are near 80°N and 64°S. Gravity waves are clearly observed in HIRDLS data via vertical temperature fluctuations in the retrieved temperature profiles. We focus on the period in 2006 from 1 to 31 May, a period covered by the initial data released for validation. Our results are based on data version 2.04.09. *Ern et al.* [2004] estimated gravity wave momentum flux from CRISTA observations, and showed that patterns in temperature variance do not well represent the distributions of gravity wave momentum flux. We present here a similar analysis of HIRDLS data, exploiting HIRDLS' higher vertical resolution and horizontal sampling.

[5] In the manuscript we discuss the measurements and our global analysis technique, and show global estimates of momentum flux magnitudes as a function of height from 20 to 60 km. The momentum flux magnitudes can be considered as lower limit constraints because the horizontal wave numbers will be systematically underestimated due to the unknown propagation directions of the waves and because of line-of-sight attenuation of wave amplitudes, particularly at high horizontal wave numbers. The global momentum flux maps clearly point to areas where large amplitude gravity wave events occur. Focusing on these areas, we find temperature fluctuations with coherent horizontal and vertical phase variations; clear evidence of well-resolved gravity wave events. These results highlight the high resolution afforded by the HIRDLS data and their value for quantifying the most urgently needed properties of gravity waves on a global scale.

2. Global Analysis of HIRDLS Temperature Profiles for Gravity Waves

2.1. HIRDLS Level 2 Temperature Data

[6] We use HIRDLS temperature profile (level 2, version v2.04.09) data as a basis for our analysis. The vertical resolution is ~0.7 km. The horizontal spacing between profiles is ~75–100 km. The spacing varies with scan rate, which has varied during the mission, but is roughly 100 km during the May 2006 period. The measurements integrate along the line of sight giving a measurement weighting function with a length of ~200 km. Perpendicular to the line of sight, the weighting function is narrow (~20 km), largely determined by the slit width. The line of sight lies at a ~47° angle from the orbit plane, so adjacent profile weighting functions do not overlap. The measurements are therefore sensitive to all waves with horizontal wavelengths longer than ~200 km for waves propagating along the line of sight (LOS) and to much shorter horizontal wavelength waves propagating perpendicular to the LOS. The measured wave amplitudes will be attenuated according to these weighting function properties, with the degree of attenuation depending on the wave vertical and horizontal wavelength and horizontal propagation direction relative to the LOS. Since the latter is unknown, we cannot correct for this attenuation, but note its presence and the consequence that the measured temperature amplitudes should generally be considered lower limits of the true wave amplitudes. The ~100 km distance between adjacent profiles determines the minimum horizontal wavelength that can be determined and that is ~200 km, but the measurements may be sensitive to, but undersample, waves with shorter horizontal wavelengths >20 km.

[7] After launch it was learned that the HIRDLS view of Earth's atmosphere is limited by an obscuration that covers much of the front aperture. Since then, the obscuration has been characterized and its radiative effects largely removed from the HIRDLS radiances [*Gille et al.*, 2005; *Barnett et al.*, 2005; *Gille et al.*, 2008]. The obscuration causes oscillations in radiance during vertical scans, which must be considered carefully prior to the wave analysis. These radiance oscillations have been carefully characterized and removed using a Singular Value Decomposition method described by *Gille et al.* [2008]. In the temperature channels, these oscillations are <1% of the magnitude of the measured atmospheric radiance before their removal, and after removal any residual is below the estimated noise levels, <0.1%. In contrast, typical wave fluctuations are ~2–5% of the atmospheric radiance, at least an order of magnitude larger than any residual obscuration oscillations.

[8] The general retrieval algorithm (Optimal Estimation [*Rodgers*, 2000]) remains largely unchanged from the prelaunch version. (See also the HIRDLS Algorithm Theoretical Basis Document, which can be found via the NASA Earth Observing System Web site at http://eospso.gsfc.nasa.gov/.) However, the retrieval scheme for temperature has been modified in an attempt to reduce the errors. In the current scheme, temperature is retrieved in two stages. In the first stage, a fast forward model [*Francis et al.*, 2006] based on the Curtis-Godson approximation is used to obtain a first guess profile for the second stage using a more accurate, regression-based forward model [*Francis et al.*, 2006] leading to the retrieved profile. The other change in the temperature retrieval has been the use of HIRDLS temperatures to define LOS temperature gradients. These have been replaced with GEOS assimilation product temperature gradients because of the required change in the latitude/longitude sampling pattern post launch. The

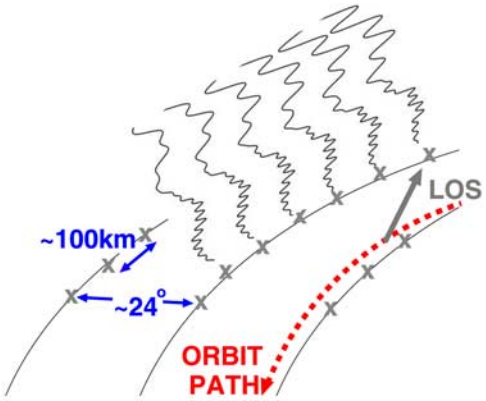

Figure 1. Schematic showing temperature perturbation profiles (fluctuating black lines) extending vertically from the HIRDLS measurement swaths (thin black arcs) along the surface of the Earth. Profile locations are marked with crosses along adjacent orbit measurement swaths, which are separated by ~24° between measurement tracks and 100 km along track. The HIRDLS line-of-sight view direction (gray arrow) is behind and to the right of the orbit track direction (dashed red arc).

HIRDLS temperature precision remains close to the prelaunch requirement of 0.4 K [*Gille et al.*, 2008]. Some biases in absolute temperature remain, but these do not affect our analysis of the wave temperature fluctuations because biases will be removed with the subtraction of the zonal mean (see section 2.3).

[9] Figure 1 is a schematic illustrating HIRDLS temperature profiles and sampling along an orbit measurement swath. We use temperature profiles as a function of pressure p. For the wave analysis, the vertical pressure grid p is converted to a pressure-altitude coordinate z using a constant 7-km scale height, so that $z = 7 \cdot \ln(p_0/p)$ with $p_0 =$ 1000 hPa. Hereafter, the term altitude refers to z. Only data on pressure levels that lie 1 km above the reported cloud-top pressure in the Level 2 files are included in the analysis to eliminate any cloud effects within a retrieval grid point scale on temperature. The upper level of retrieved temperatures lies at 64.5 km. The top few levels of v2.04.09 have higher noise (R. Khosravi, personal communication, 2007). We exclude data above 60 km from our analysis and show wavelet analysis results up to 55 km altitude.

2.2. S Transform Analysis

[10] Our wave analysis technique uses the S transform [*Stockwell et al.*, 1996], a spectral analysis technique similar to a continuous wavelet analysis, that provides both the spectral properties of the signal as well as the spatial variations in those spectral properties. The S transform basis functions are formed as the product of sinusoidal functions modulated by a Gaussian with width inversely proportional to the wavelength. The spatial integral of the S transform gives the Fourier transform. The Gaussian is translated along the spatial dimension to give the localization of spectral information, while the phase remains fixed relative to a single position. We have previously applied the S transform for gravity wave analysis by *Wang et al.* [2006].

[11] To illustrate the S transform analysis, we have defined a set of six synthetic temperature perturbation profiles $T'(z)$ (shown in Figure 1) as the sum of three wave oscillation patterns with three different vertical wavelengths and amplitude variations with height:

$$T'(z) \sum_{j=1,3} A_j \sin\left(2\pi m_j z + \phi_j\right), \quad (1)$$

where $m_1 = 0.5$ km^{-1}, $m_2 = 0.2$ km^{-1}, $m_3 = .05$ km^{-1}. The amplitudes are given by $A_1 = (2.5\ \text{K})\exp[-(z-z_1)^2/\ln 2/(20\ \text{km})^2]$ with $z_1 = 20$ km, $A_2 = \exp[(z-z_2)/7\ \text{km}]$ with $z_2 =$ 35 km, and $A_3 = 5$ K. For adjacent profiles, the phase shifts by $\Delta\phi_1 = \pi/3$, $\Delta\phi_2 = 3\pi/2$, $\Delta\phi_3 = \pi/12$. With 100-km spacing between profiles, these correspond to horizontal wave numbers $k_1 = 2\pi/600$ km, $k_2 = 2\pi/133$ km, $k_3 = 2\pi/2400$ km. Figure 2 shows the wavelet transform amplitude spectrum versus altitude for the profiles shown in Figure 1. The S transform clearly identifies the three wave signals and their variability in height. The $m_2 = 0.2$ km^{-1} wave signal suffers from wraparound effects seen at the bottom of the profile where the true signal has negligible amplitude. Our HIRDLS analysis employs zero padding of the profiles to prevent this wraparound effect.

[12] The S transform also includes information on wave phase versus vertical wavelength and height. Figure 3 shows the analysis of the six profiles along the sample path in Figure 1. The horizontal wavelength variations given to these synthetic profiles appear as variations in phase from profile to profile. The phase changes are undersampled for the wave with $\Delta\phi_2 = 3\pi/2$ in the center panel, such that the horizontal wavelength derived from the analysis, $2\pi\Delta x/\Delta\phi = 400$ km, is much longer than the true horizontal wavelength = 133 km.

2.3. Gravity Wave Analysis

[13] The global array of HIRDLS profiles included in each day of measurements are analyzed by first computing the zonal mean temperature as a function of altitude and latitude, in 2.5° bins. We next compute planetary-scale

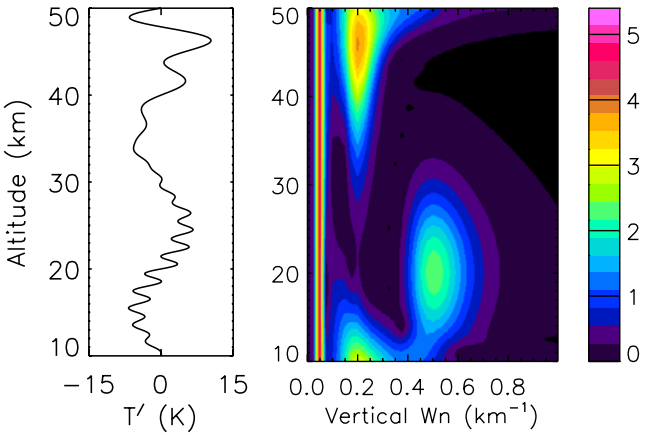

Figure 2. (left) Synthetic temperature perturbation profile and (right) its S transform amplitude spectrum versus height. The color scale represents amplitude in °K. The S transform clearly captures the three wave signals input to create the profile and their variability in height.

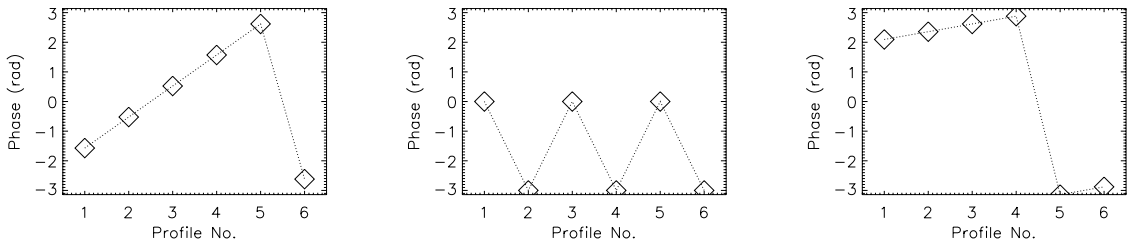

Figure 3. Phase as a function of profile number at the maximum amplitude height for the three wave signals: (left) ϕ_1, (middle) ϕ_2, (right) ϕ_3 identified in Figures 1 and 2.

zonal oscillations from the remaining longitudinal variations. We perform S transform analysis on the data interpolated to constant longitude resolution of 24°. The transform includes amplitude and phase of wave numbers 1–7 as a function of longitude. Wave numbers 1 and 2 dominate at most latitudes and heights, and wave number 3 becomes prominent in some regions during a portion of the month. Higher wave numbers have weak amplitude during this month, and they are poorly resolved, so we use wave numbers 0–3 here to define the "large-scale temperature" for subtraction from the HIRDLS temperatures to determine the perturbation profiles.

[14] The S transform is next computed in altitude for each temperature perturbation profile. The resulting transform $\tilde{T}$ (z, λ_Z) is a complex-valued function of altitude z and vertical wavelength λ_Z. For each adjacent profile pair (i, i + 1), the cospectrum $C_{i,i+1}$ is computed,

$$C_{i,i+1} = \tilde{T}_i \tilde{T}^*_{i+1} = \hat{T}_i \hat{T}_{i+1} e^{i\Delta\phi_{i,i+1}}, \tag{2}$$

where $\hat{T}_i$ is the amplitude and $\Delta\phi_{i,i+1}$ is the phase shift between adjacent profiles i and i + 1. The covariance spectrum is the absolute value $|C_{i,i+1}|$. We locate the maximum in the covariance spectrum for vertical wavelengths less than 16 km and record the vertical wavelength at the maximum as a function of altitude. The depth of the profile useful for our analysis is generally 40 km (from 20 to 60 km). For the S transform analysis, we zero pad the profiles between the surface and 20 km and between 60 and 70 km at the top. We chose a vertical wavelength cutoff at 16 km to focus on shorter vertical wavelength signals that will be minimally affected by the zero padding.

[15] The covarying amplitude $\hat{T}_{i,i+1}(z,\lambda_Z)$ and phase difference $\Delta\phi_{i,i+1}(z,\lambda_Z)$ are computed as

$$\hat{T}_{i,i+1} = \sqrt{|C_{i,i+1}|} \tag{3}$$

$$\Delta\phi_{i,i+1} = \tan^{-1}\left(\frac{\mathrm{Im}(C_{i,i+1})}{\mathrm{Re}(C_{i,i+1})}\right). \tag{4}$$

[16] The result gives the wave amplitude, vertical wavelength, and horizontal phase shift of the largest amplitude wave present in both profiles. From the horizontal phase shift $\Delta\phi_{i,i+1}$, we estimate the horizontal wave number k_H along the line joining the two profiles via

$$k_H = \Delta\phi_{i,i+1}/\Delta r_{i,i+1}, \tag{5}$$

where $\Delta r_{i,i+1}$ is the horizontal distance between the two profiles. This horizontal wave number will in general be an underestimate of the true horizontal wave number since the orientation of segment of length $\Delta r_{i,i+1}$ joining adjacent profiles will in general lie at some angle relative to the wave propagation direction. The horizontal variations may also be undersampled. The horizontal wavelengths we derive with this procedure are therefore necessarily only an estimate, and will generally be an overestimate of the true horizontal wavelength or an underestimate of the true horizontal wave number. *Ern et al.* [2004] showed evidence for substantial undersampling in their CRISTA analysis at high latitudes. Our horizontal sampling is a factor of 2.4 better than CRISTA, but some undersampling is still expected.

[17] The S transform cospectral analysis of adjacent profile pairs therefore gives temperature amplitude, vertical wavelength, and an estimate of horizontal wavelength along the orbit measurement track direction as a function of height for each profile pair. From these local estimates of wave properties we can estimate the momentum flux $M_{i,i+1}$.

$$M_{i,i+1} = \frac{\rho}{2}\lambda_z \frac{k_H}{2\pi}\left(\frac{g}{N}\right)^2\left(\frac{\hat{T}_{i,i+1}}{T}\right)^2, \tag{6}$$

where ρ is the background density, g is Earth's gravitational acceleration, N is the buoyancy frequency, and T is the background temperature that includes wave numbers 0–3. This momentum flux is an absolute value, and contains no information on the propagation direction of the waves. Because k_H is generally an underestimate of the true wave number, $M_{i,i+1}$ will be correspondingly underestimated.

2.4. Results

[18] We have performed this analysis on all adjacent profile pairs for 30 d of HIRDLS measurements and have computed global maps of wave properties. In Figure 4 we show results binned in 5° latitude × 30° longitude bins and averaged over the 30 d and over 20–30 km altitude. These results include vertical wavelengths <16 km. The theoretical minimum vertical wavelength from HIRDLS is ~2 km. The upper left panel shows temperature amplitude; the upper right panel shows momentum flux; the lower left panel shows vertical wavelength; and the lower right panel shows horizontal wave number.

[19] To estimate the effects of noise on these results, we performed this analysis on a set of random temperature perturbations with standard deviation of 0.5 K. This analysis results in featureless maps with temperature amplitude 0.36 K, vertical wavelength 2.2 km, horizontal wavelength

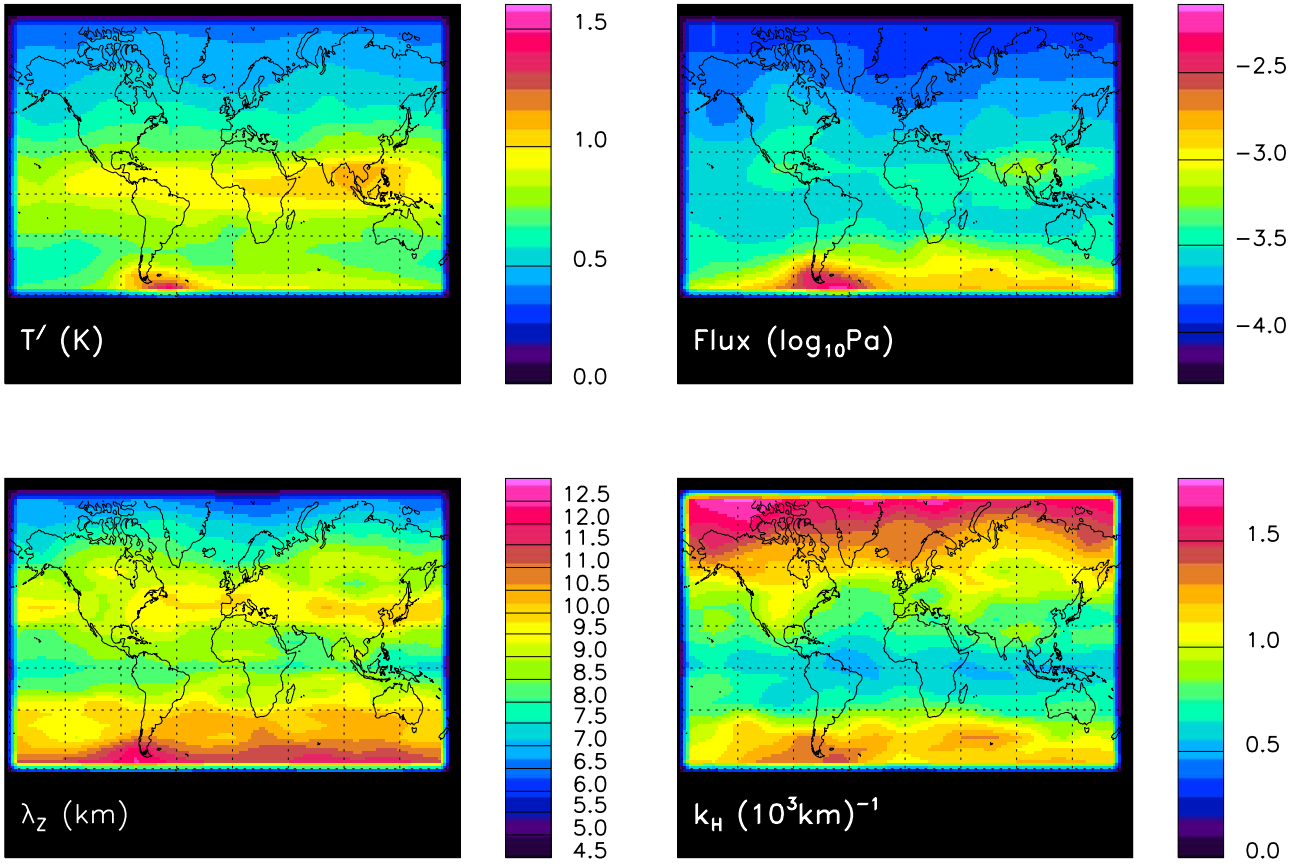

Figure 4. Maps of gravity wave properties derived from HIRDLS averaged over 30 d in May 2006 and averaged over the height range 20–30 km. (top left) Wave temperature amplitude (T'); (top right) momentum flux (flux); (bottom left) vertical wavelength (λ_Z); (bottom right) horizontal wave number (k_H).

400 km (2.5 in units $(10^3\ \mathrm{km})^{-1}$ as plotted in Figure 4), and momentum flux 3×10^{-5} Pa. The results in Figure 4 do not reach these values anywhere, but show a trend of approaching these limits at the highest latitudes in the northern (summer) hemisphere.

[20] Figure 4 includes wave events for days 121–151 (1–31 May) in 2006 (day 143 is missing in the v2.04.09 data set). The results in these maps represent the analysis of 166,690 profile pairs. The top left temperature amplitude map can be compared to previous satellite data analyses of gravity wave temperature variance. The patterns are very similar to previous results from LIMS [*Fetzer and Gille*, 1994] and CRISTA [*Preusse et al.*, 2002; *Ern et al.*, 2004]. Both of these were limb-viewing infrared instruments, and the analysis techniques included a wide range of vertical wavelengths, although HIRDLS can observe shorter vertical wavelengths. Like these previous analyses, we can see winter/summer asymmetries in temperature amplitudes at mid and high latitudes, with larger average amplitude waves in winter. Our May averages, although it is late fall rather than winter in the southern hemisphere, show similar features as the CRISTA data from August. (Our May mean map of temperature amplitude in general shows patterns similar to previous southern hemisphere winter data.) There is also a band of enhanced temperature amplitude in the equatorial region.

[21] The HIRDLS temperature amplitude map also has some features similar to maps of gravity wave potential energy derived from short vertical scale variance in temperature profiles derived from GPS occulation measurements [*Tsuda et al.*, 2000; *Ratnam et al.*, 2004; *de la Torre et al.*, 2006] and radiosondes [*Allen and Vincent*, 1995]. Both techniques included only short vertical wavelength waves, <10 km for GPS and <7 km for the radiosonde analysis. These two data sets both show peak wave energies in the tropics in the lower stratosphere, similar to Figure 4. They also show seasonal asymmetry at higher latitudes, with larger values in winter, although the increase with latitude in winter is much weaker than in HIRDLS where long vertical wavelengths that were excluded in the previous studies occur.

[22] For quantitative comparison, peak values in equatorial potential energy shown by *Tsuda et al.* [2000] can be converted to an average temperature amplitude [see *Alexander and Barnet*, 2007] to give a value of ~2 K. Temperature variances derived from equatorial rocketsondes averaged over a slightly higher altitude range (20–40 km) [*Eckermann*, 1995] suggest similar average temperature amplitudes ~1.8–1.9 K during the May

season. Figure 4 shows somewhat lower peak equatorial values of 1.25 K, approximately 60% lower. This lower value may be due in part to the poorer vertical resolution of HIRDLS compared to GPS. Effects of vertical resolution on GPS wave amplitudes can be inferred from the results of *de la Torre et al.* [2006].

[23] Differences may also be due in part to the analysis method. The GPS and sonde studies did not remove the large scale-zonal waves, but relied on a vertical filter to select for short vertical wavelengths. However, global-scale Kelvin waves have been observed with vertical wavelengths as short as 3–4.5 km [*Holton et al.*, 2001], so these may contribute in part to the larger equatorial temperature amplitudes in the GPS and radiosonde studies. For better comparison to the GPS and sonde results, we computed simple HIRDLS temperature variance without the removal of zonal wave numbers 1–3 (not shown), and peak amplitudes derived from this variance near the equator were then 2.0 K. Comparing our analyzed equatorial wave amplitudes with and without the removal of wave numbers 1–3, the large-scale waves account for a 25–30% difference in amplitude, about half of the difference. The other 30% is due to our covariance analysis method, which demands that coherent temperature fluctuations exist in neighboring profiles. These combined effects bring the HIRDLS temperature amplitudes into very close agreement with previous measurements of short vertical wavelength waves in the tropics.

[24] Temperature variance maps derived from the Upper Atmosphere Research Satellite-Microwave Limb Sounder (UARS-MLS) [*Wu and Waters*, 1996a; *McLandress et al.*, 2000] included only long vertical wavelength waves >12 km [*Alexander*, 1998], and these maps show the large increase at high latitudes in the winter hemisphere but do not show a peak at the equator. Average temperature amplitudes derived from the UARS-MLS data [see *Alexander and Barnet*, 2007] are very small ~0.2 K and likely explained by the combined effects of weighting function attenuation and intermittency on the average.

[25] Comparison of the top left and top right panels in Figure 4 illustrate differences in the patterns of temperature amplitude and momentum flux. In general, the main difference can be traced to differences in wave horizontal and vertical wavelength. The equatorial waves tend to have shorter vertical wavelength and lower horizontal wave number than the high-latitude waves. These trends systematically lead to smaller momentum fluxes in the equatorial region compared to higher latitudes according to (6). A similar result and cause were also noted by *Ern et al.* [2004]. Note the location of largest momentum fluxes near the tip of South America.

[26] Comparing these results to maps derived from CRISTA observations [*Ern et al.*, 2004], the patterns in temperature amplitude, horizontal wave number, and momentum flux are qualitatively very similar. Vertical wavelength from CRISTA displayed no obvious global trends [*Ern et al.*, 2004], whereas the HIRDLS results show a distinct trend with increasing vertical wavelength from the equator to high latitudes in the southern (winter) hemisphere. *Ern et al.* [2004] analyzed data from August 1997, while our HIRDLS results are for May 2006. The seasons are similar, but not identical. This could account for some differences, but would not likely explain the primary difference observed near the equator. The CRISTA and HIRDLS analyses used different maximum wavelength cutoffs, 30 and 16 km, respectively, which might explain some differences. The differences in the vertical wavelength latitudinal trends between CRISTA and HIRDLS might also simply be due to the higher vertical resolution of HIRDLS compared to CRISTA. The results reported by *Ern et al.* [2004] had vertical resolution of 3 km. The improved vertical resolution of the HIRDLS data may mean they simply include more of the short vertical scale waves known to exist in the equatorial region. The previously discussed observational analyses of only short vertical wavelengths less than ~10 km have shown peaks in amplitude near the equator [*Tsuda et al.*, 2000; *Alexander et al.*, 2002], whereas analyses that included only long vertical wavelength waves show peaks in the winter extratropics and summer subtropics [*Wu and Waters*, 1996a; *Alexander*, 1998]. HIRDLS, with its high vertical resolution that extends over a deep region of the atmosphere, can clearly observe both types of waves.

[27] The maximum horizontal wave numbers in Figure 4 correspond to a horizontal wavelength of ~500 km, and they occur at high latitudes. As explained by *Ern et al.* [2004], in regions where waves are undersampled in the horizontal, a horizontal wavelength = $4\Delta r_{ij}$ or ~400 km would be expected to appear in the mean. Figure 5 shows histograms of gravity wave horizontal wave number in three latitude bands for comparison to histograms shown by *Ern et al.* [2004]. These are derived from 1 d of measurements (>5500 profile pairs). The waves identified in our HIRDLS analysis do not show the flattened distribution that indicated severe undersampling in CRISTA at high latitudes [*Ern et al.*, 2004]. Although undersampling is likely for some of the waves in the HIRDLS maps, it does not appear to be a pervasive issue. The "noise" distribution (Figure 5) has a distinctly different shape than the observations, showing a broad peak centered at $k_H = 2.5$ $(10^3$ km$)^{-1}$, the 400-km horizontal wavelength predicted by the *Ern et al.* [2004] formula.

[28] Quantitative differences between CRISTA and HIRDLS may have numerous origins. For vertical wavelength and horizontal wave number, the differing resolution of the two data sets will tend to allow HIRDLS to see a larger portion of the wave spectrum than CRISTA, and we expect to see a decrease in the minimum vertical wavelength and increase in the maximum k_H, as observed. For temperature amplitudes, the data processing methods also include significant differences that would also be likely to affect the quantitative comparison. *Ern et al.* [2004] used an amplitude correction to attempt to account for the radiative transfer attenuation of the measurement, in particular the reduction in amplitude associated with the measurement weighting function. We instead chose not to apply such a correction because, as explained in section 2, it depends not only on the known weighting function of the measurements and the observed vertical wavelength but also on the unknown wave propagation directions. Such corrections can therefore in some cases increase the error in wave amplitudes. Instead, our analysis without correction will reliably represent a lower limit on the wave amplitudes beyond the small effects of measurement noise. Horizontal

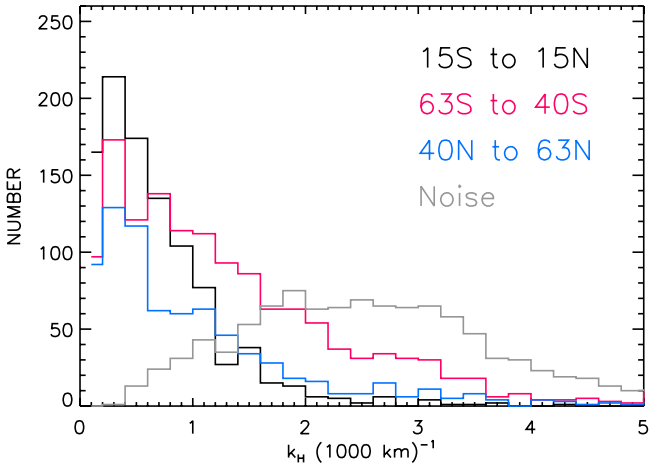

Figure 5. Distribution of gravity wave horizontal wave number (averaged over the altitude range 20–30 km) in three latitude bands. The gray histogram shows the distribution obtained from analysis of random noise.

wave numbers will also generally be underestimated by our analysis as explained in section 2.3. As a result, momentum flux from our analysis will represent a reliable lower limit apart from the small effects of measurement noise estimated at $\sim 10^{-5}$ Pa. Another difference between our analysis of HIRDLS and that of CRISTA lies in the vertical wavelength matching criterion between adjacent profiles prior to determination of the horizontal wave number. For CRISTA, a

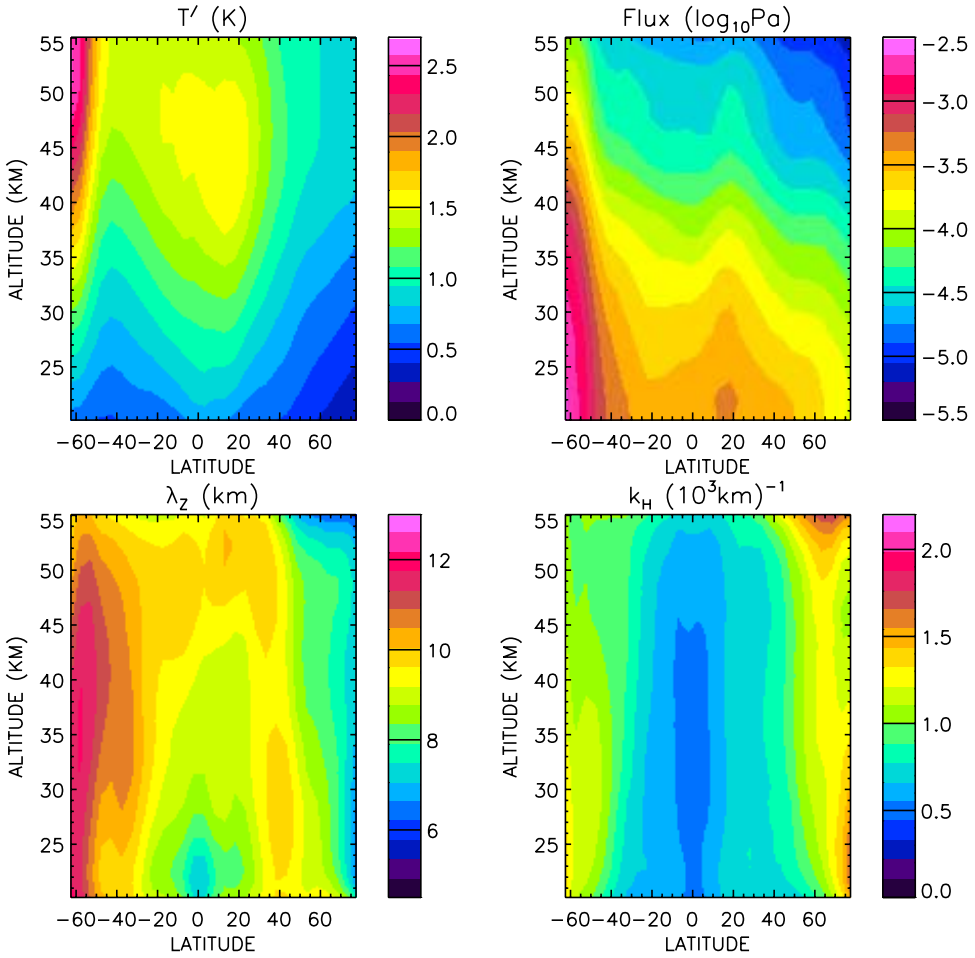

Figure 6. Latitude height variations in gravity wave properties. (top left) Wave temperature amplitude (T'); (top right) momentum flux (flux); (bottom left) vertical wavelength (λ_Z); (bottom right) horizontal wave number (k_H).

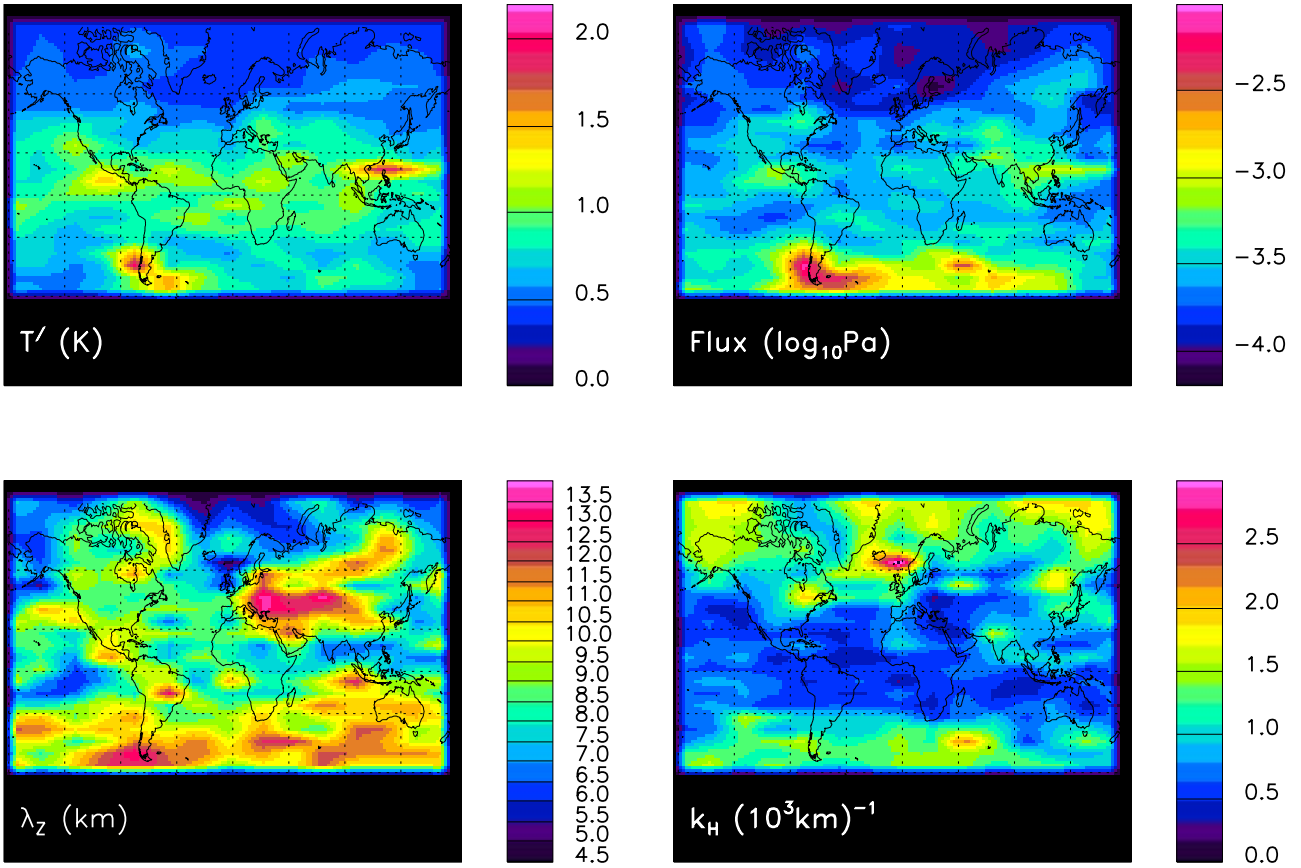

Figure 7. Maps of gravity wave properties averaged over 20–30 km as in Figure 4 for the single day 16 May 2006.

looser matching criterion was applied that required the vertical wavelength in the two profiles differ by less than 6 km, and the amplitude was determined as the average of the two amplitudes in adjacent profiles. In contrast, by using the spectral covariance and phase shift from the S transform, wave identification and matching is performed in the spectral domain so that exact vertical wavelength matching within the resolution of the S transform is assured. This difference could tend to decrease the number of wave events we observe, but the high resolution and longer duration of the HIRDLS mission leave an abundance of wave events to study even with our stricter criterion.

[29] Figure 6 shows zonal means of temperature amplitude, momentum flux, vertical wavelength and horizontal wave number as functions of latitude and height. In this view, it is very clear that the equatorial maximum in the temperature amplitude that has been seen in other temperature variance data sets from limb sounding satellite instruments [*Fetzer and Gille*, 1994; *Tsuda et al.*, 2000; *Preusse et al.*, 2001] is not present in the momentum flux. In the flux we instead see a local minimum near the equator and maxima at higher latitude in the winter hemisphere and in the subtropics in summer. In the ECHAM4 model experiments of *Manzini and McFarlane* [1998] and *Giorgetta et al.* [2002], which gave realistic middle atmosphere circulations, the parameterized gravity wave momentum flux at the tropopause was also a local minimum at the equator. Values of the parameterized wave momentum flux near the tropopause at the equator and extratropical in the winter hemisphere in these model studies had values similar to those in Figure 6.

[30] The latitudinal variations in amplitude, vertical wavelength, and horizontal wave number remain fairly constant with height up to ~40–45 km altitude. Vertical wavelengths show increases with height between latitudes 60°S and 30°N [*Smith et al.*, 1987]. Above 50 km in the northern (summer) hemisphere, there is a dramatic decrease in vertical wavelength and increase in horizontal wave number. Here the amplitudes are also small, and the analysis may be showing the properties of noise.

[31] Figure 6 shows that temperature amplitudes grow with height, but significantly less than the theoretical growth in the absence of dissipation of a factor of $\exp(\Delta z/2H) \sim 4$ between 25 and 45 km. Dissipation would be consistent with a decrease in momentum flux at the higher altitudes, and indeed momentum fluxes at 45 km have decreased to about 10–20% of their values at 25 km, suggesting substantial dissipation and mean-flow forcing. However, we cannot compute the mean-flow forcing from these results: without additional knowledge of the propagation directions of the waves and how the observational vertical wavelength filter may be affecting the observed fluxes [*Alexander*, 1998]. Instead, these results can be used to constrain models and parameterizations of gravity wave mean-flow forcing (see section 3).

[32] Figure 7 shows maps of wave properties averaged over 20–30 km altitude as in Figure 4 but for a single day

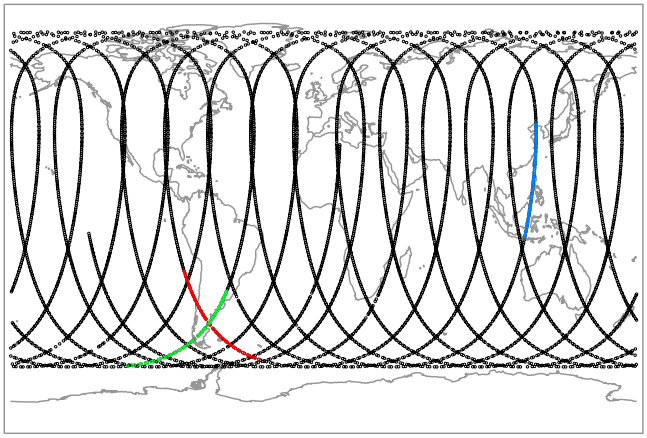

Figure 8. Map showing the location of HIRDLS profiles measured on 16 May 2006 (open circles) and segments that are highlighted in Figures 9 and 10. The ascending and descending segments over America are distinguished via red and green, respectively. The descending segment over Southeast Asia is shown in blue.

(16 May 2006). Similar global patterns in temperature amplitude, momentum flux, vertical wavelength, and horizontal wave number appear in both the 30-d mean (Figure 4) and single day (Figure 7), although single days show localized spots of wave activity and a higher degree of spatial variability.

[33] The localized spots of enhanced temperature amplitude and momentum flux in Figure 7 are associated with isolated strong wave events. We next focus on two regions of enhanced temperature amplitude, over the South American Andes and over Southeast Asia, to illustrate such events. Figure 8 shows the locations of individual HIRDLS profiles on day 136. Three segments are overplotted in color where the series of profiles will be shown as cross sections in Figures 9 and 10.

[34] Figure 9 shows temperature perturbation profiles along the descending orbit segment over Southeast Asia (blue segment in Figure 8). A wave-like feature with vertical wavelength of ~6 km appears at 17° latitude and at 17–50 km. Also plotted for reference are cloud-top heights (in km) below the measurement swath at 0600 UT derived from geostationary infrared cloud imagery. The time of the cloud data corresponds to ~1 h prior to the HIRDLS measurement. The wave event is likely generated by deep convection. Note that the wave event does not show any clear phase tilt with latitude, and therefore the along-track k_H derived from the global analysis is very long ~1/10,000 km. If the true propagation direction of this wave is instead zonal, the true horizontal wave number may be much higher, and the momentum flux in our analysis could be severely underestimated. For example, if this is a zonally propagating wave number = 10 wave, the momentum flux would be underestimated by a factor of 2.5.

[35] We also highlight two segments over the Patagonian Andes mountains in Figure 10. These segments are shown as red and green (for ascending and descending, respectively) in the southern hemisphere in Figure 8. This is a region where CRISTA, UARS-MLS, and AIRS and AMSU-A have previously detected large wave temperature variance [*Eckermann and Preusse*, 1999; *Preusse et al.*, 2002; *Ern et al.*, 2004; *Wu and Waters*, 1996a, 1996b; *McLandress et al.*, 2000; *Wu*, 2004; *Jiang et al.*, 2002; *Alexander and Barnet*, 2007; *Alexander and Teitelbaum*, 2007]. Figure 10 shows the series of temperature perturbation profiles as a function of distance along these segments from west to east (left to right). In both cases, westward tilting phase surfaces with height indicate westward and upward intrinsic group velocity, with amplitudes increasing with height above the Andes topography. These are mountain waves that can be seen to propagate into the mesosphere above 50 km. These waves are commonly observed in HIRDLS data in this region of the world. Note that the local wave amplitudes exhibited in Figures 9 and 10 are much larger than the longitude/latitude binned values in the maps of Figures 4 and 7 or in the zonal mean (Figure 6) because of spatial and temporal

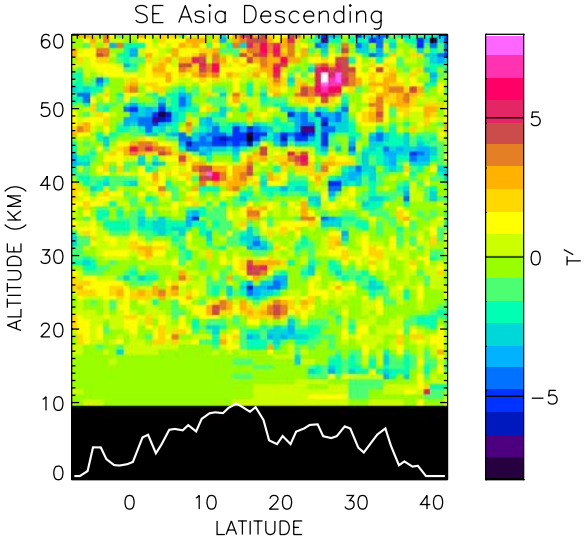

Figure 9. Temperature perturbation (K) profiles plotted along the segment over southeast Asia (see Figure 8). Also plotted (white line) are cloud top heights below the measurements ~1 h prior to the HIRDLS measurements. Cloud top heights are derived from the NOAA/NCDC global infrared data set.

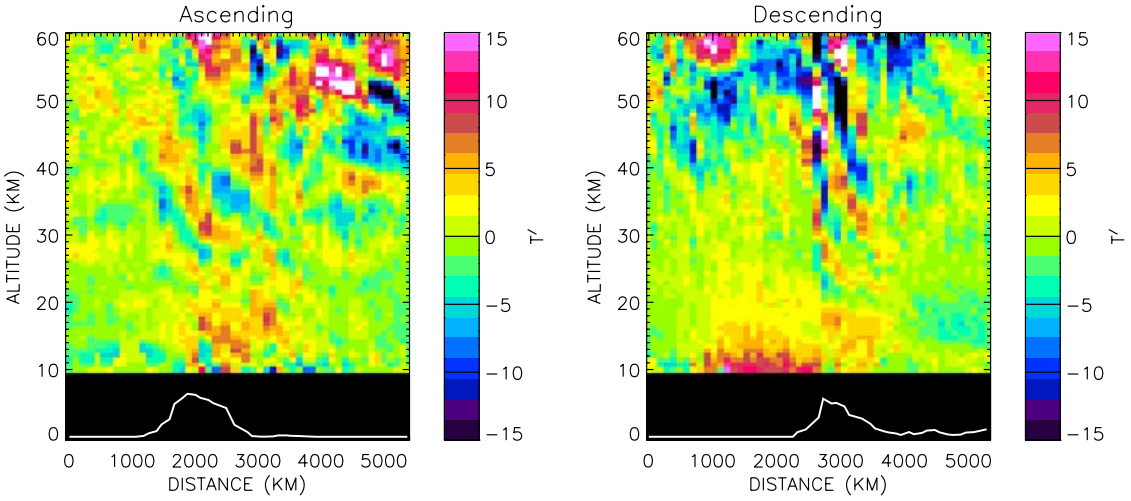

Figure 10. Temperature perturbation (K) profiles along the ascending and descending segments over South America (see Figure 8) plotted as a function of horizontal distance and altitude. The distances are measured from west to east along the segments. Also plotted (white line) are topographic heights (in km exaggerated by a factor of 5). Topographic heights are from NCEP 2.5° orography.

intermittency. Although the wave features in Figures 9 and 10 suggest wave observations would still benefit from an instrument with even better resolution that HIRDLS, these results show some tantalizing two-dimensional detail that is unique among the available satellite data sets.

3. Discussion and Summary

[36] We describe a global analysis of HIRDLS high-resolution temperature profile data to derive properties of gravity waves. We derive simultaneous estimates of temperature amplitude, vertical wavelength, and horizontal wave number which allow calculation of wave momentum fluxes. The determination of horizontal wave number is the most uncertain of the properties, and the wave number will nearly always be underestimated, sometimes substantially, because of horizontal sampling of the measurements. This uncertainty makes the derived momentum flux a lower limit of the true value. Wave propagation is not determined with our method. The results therefore provide a lower bound on the absolute value of wave momentum fluxes. The lack of information on wave propagation directions means we cannot compute mean-flow forcing from the vertical gradients in momentum flux shown in Figure 6. However, observations of individual gravity wave events such as those shown in Figure 10 can be used to constrain models of gravity wave generation and propagation and can also constrain parameterizations of gravity waves in general circulation models. In these ways the observations can be used to constrain parameterized gravity wave mean-flow forcing effects in general circulation models.

[37] The wave properties show substantial variations in latitude. Variations in temperature amplitude, horizontal wave number, and momentum flux resemble those seen in previous analyses of radiosondes [*Wang et al.*, 2005] and CRISTA [*Ern et al.*, 2004], but with quantitative differences likely associated with the resolution of the different data sets. The vertical wavelength distributions in HIRDLS show substantial variations with latitude not previously seen in other data sets. The reason for the new result is likely associated with the high vertical resolution of HIRDLS and the deep region of observation up to 60-km altitude, both of which allow the determination of a wider range of vertical wavelengths not possible in previous analyses.

[38] The momentum fluxes we derive show a local minimum near the equator, largest values at high latitudes in the late fall season in the southern hemisphere, and smaller but significant values at summer subtropical latitudes (∼20N). In addition to the uncertainties described above, the momentum fluxes and their global distributions are likely to be affected by the limitations of the measurements and analysis. In particular, we determine momentum fluxes only for waves with vertical wavelengths in the range 2–16 km. We should further note that HIRDLS sensitivity to the shortest vertical wavelengths in this range remains to be determined. Undersampling of short horizontal wavelength waves in the HIRDLS data is another issue that could result in systematic biases in horizontal wave number and momentum flux with latitude. For example, if high horizontal wave number gravity waves have a preference for zonal propagation directions, then the HIRDLS sampling would favor their characterization at the high-latitude limits of the measurements and would result in gross underestimates of horizontal wave number and momentum flux at low latitudes. Conversely, a meridional propagation preference would favor characterization at low latitudes. One low-latitude case study (Figure 9) described in section 2.4 indicated a possible underestimate of momentum flux by a factor of 2.5, and even larger underestimates are possible.

[39] Maps of wave properties derived from individual days of measurements show similar patterns as seen in the 30-d average maps, but they contain isolated patches of varying wave properties that can be traced to local wave events in the data. We show examples of waves likely generated by convection and flow over mountains. These illustrate that the patchy appearance of these daily maps is not due to noise in the data, but instead show real intermittency in gravity wave occurrence and wave properties. The

global gravity wave analysis technique we describe reliably highlights the locations of these intermittent wave events.

[40] The HIRDLS data set represents a very valuable information source on the global properties of gravity waves that we have only begun to exploit. Despite their limitations, these data hold the potential to greatly constrain the properties of waves specified in GCM parameterizations of gravity wave mean-flow forcing effects, which are currently severely underconstrained.

[41] **Acknowledgments.** M.J.A.'s work was funded by National Aeronautics and Space Administration (NASA) Aura Validation contract NNH06CD16C. Coauthors at the University of Colorado were supported by NASA under contract NAS5-97046. The National Center for Atmospheric Research is sponsored by the National Science Foundation. Work at the Jet Propulsion Laboratory, California Institute of Technology, was carried out under a contract with NASA. HIRDLS is funded by NASA in the United States and by the Natural Environment Research Council in the UK.

References

Alexander, M. J. (1998), Interpretations of observed climatological patterns in stratospheric gravity wave variance, *J. Geophys. Res.*, *103*(D8), 8627–8640.

Alexander, M. J., and C. Barnet (2007), Using satellite observations to constrain gravity wave parameterizations for global models, *J. Atmos. Sci.*, *64*(5), 1652–1665.

Alexander, M. J., and H. Teitelbaum (2007), Observation and analysis of a large amplitude mountain wave event over the Antarctic peninsula, *J. Geophys. Res.*, *112*, D21103, doi:10.1029/2006JD008368.

Alexander, M. J., T. Tsuda, and R. A. Vincent (2002), On the latitudinal variations observed in gravity waves with short vertical wavelengths, *J. Atmos. Sci.*, *59*, 1394–1404.

Allen, S. J., and R. A. Vincent (1995), Gravity wave activity in the lower atmosphere: Seasonal and latitudinal variations, *J. Geophys. Res.*, *100*(D1), 1327–1350.

Barnett, J. J., C. L. Hepplewhite, L. Rokke, and J. C. Gille (2005), Mapping the optical obscuration in the NASA Aura HIRDLS instrument, *Proc. SPIE*, *5883*, 58830I, doi:10.1117/12.623574.

de la Torre, A., T. Schmidt, and J. Wickert (2006), A global analysis of wave potential energy in the lower stratosphere derived from 5 years of GPS radio occultation data with CHAMP, *Geophys. Res. Lett.*, *33*, L24809, doi:10.1029/2006GL027696.

Eckermann, S. D. (1995), On the observed morphology of gravity-wave and equatorial-wave variance in the stratosphere, *J. Atmos. Terr. Phys.*, *57*, 105–134. (Corrigendum, *J. Atmos. Terr. Phys.*, *57*(6), 1)

Eckermann, S. D., and P. Preusse (1999), Global measurements of stratospheric mountain waves from space, *Science*, *286*(5444), 1534–1537.

Eckermann, S. D., et al. (2006), Imaging gravity waves in lower stratospheric AMSU-A radiances. part 2: Validation case study, *Atmos. Chem. Phys.*, *6*, 3343–3362.

Ern, M., P. Preusse, M. J. Alexander, and C. D. Warner (2004), Absolute values of gravity wave momentum flux derived from satellite data, *J. Geophys. Res.*, *109*, D20103, doi:10.1029/2004JD004752.

Ern, M., P. Preusse, and C. D. Warner (2006), Some experimental constraints for spectral parameters used in the Warner and McIntyre gravity wave parameterization scheme, *Atmos. Chem. Phys.*, *6*, 4361–4381.

Fetzer, E. J., and J. C. Gille (1994), Gravity wave variance in LIMS temperatures. part I: Variability and comparison with background winds, *J. Atmos. Sci.*, *51*, 2461–2483.

Francis, G. L., D. P. Edwards, A. Lambert, C. M. Halvorson, J. M. Lee-Taylor, and J. C. Gille (2006), Forward modeling and radiative transfer for the NASA EOS-Aura High Resolution Dynamics Limb Sounder (HIRDLS) instrument, *J. Geophys. Res.*, *111*, D13301, doi:10.1029/2005JD006270.

Gille, J., et al. (2005), Development of special corrective processing of HIRDLS data and early validation, *Proc. SPIE*, *5883*, 58830H, doi:10.1117/12.622590.

Gille, J., et al. (2008), The High Resolution Dynamics Limb Sounder (HIRDLS): Experiment overview, results and temperature validation, *J. Geophys. Res.*, doi:10.1029/2007JD008824, in press.

Giorgetta, M. A., E. Manzini, and E. Roeckner (2002), Forcing of the quasi-biennial oscillation from a broad spectrum of atmospheric waves, *Geophys. Res. Lett.*, *29*(8), 1245, doi:10.1029/2002GL014756.

Holton, J. R., M. J. Alexander, and M. T. Boehm (2001), Evidence for short vertical wavelength Kelvin waves in the Department of Energy-Atmospheric Radiation Measurement Nauru99 radiosonde data, *J. Geophys. Res.*, *106*(D17), 20,125–20,129.

Jiang, J. H., D. L. Wu, and S. D. Eckermann (2002), Upper Atmosphere Research Satellite (UARS) MLS observation of mountain waves over the Andes, *J. Geophys. Res.*, *107*(D20), 8273, doi:10.1029/2002JD002091.

Manzini, E., and N. McFarlane (1998), The effect of varying the source spectrum of a gravity wave parameterization in a middle atmosphere general circulation model, *J. Geophys. Res.*, *103*(D24), 31,523–31,539.

McLandress, C., M. J. Alexander, and D. L. Wu (2000), Microwave Limb Sounder observations of gravity waves in the stratosphere: A climatology and interpretation, *J. Geophys. Res.*, *105*(D9), 11,947–11,967.

Preusse, P., S. D. Eckermann, and D. Offermann (2000), Comparison of global distributions of zonal-mean gravity wave variance inferred from different satellite instruments, *Geophys. Res. Lett.*, *27*(23), 3877–3880.

Preusse, P., G. Eidmann, S. D. Eckermann, B. Schaeler, R. Spang, and D. Offermann (2001), Indications of convectively generated gravity waves in CRISTA temperatures, *Adv. Space Res.*, *27*(10), 1653–1658.

Preusse, P., A. Dörnbrack, S. D. Eckermann, M. Riese, B. Schaeler, J. T. Bacmeister, D. Broutman, and K. U. Grossmann (2002), Space-based measurements of stratospheric mountain waves by CRISTA: 1. Sensitivity, analysis method, and a case study, *J. Geophys. Res.*, *107*(D23), 8178, doi:10.1029/2001JD000699.

Ratnam, M., G. Tetzlaff, and C. Jacobi (2004), Global and seasonal variations in stratospheric gravity wave activity deduced from the CHAMP/GPS satellite, *J. Atmos. Sci.*, *61*(13), 1610–1620.

Rodgers, C. D. (2000), *Inverse Methods for Atmospheric Sounding: Theory and Practice*, 256 pp., World Sci., London.

Smith, S., D. Fritts, and T. VanZandt (1987), Evidence for a saturated spectrum of atmospheric gravity waves, *J. Atmos. Sci.*, *44*, 1404–1410.

Stockwell, R. G., L. Mansinha, and R. P. Lowe (1996), Localisation of the complex spectrum: The S-transform, *IEEE Trans. Signal Processes*, *44*(4), 998–1001.

Tsuda, T., M. Nishida, C. Rocken, and R. H. Ware (2000), A global morphology of gravity wave activity in the stratosphere revealed by the GPS occultation data (GPS/MET), *J. Geophys. Res.*, *105*(D6), 7257–7274.

Wang, L., M. A. Geller, and M. J. Alexander (2005), Spatial and temporal variations of gravity wave parameters. part 1: Intrinsic frequency, wavelength, and vertical propagation direction, *J. Atmos. Sci.*, *62*, 125–142.

Wang, L., M. Alexander, T. Bui, and M. Mahoney (2006), Small-scale gravity waves in ER-2 MMS/MTP wind and temperature measurements during crystal-face, *Atmos. Chem. Phys.*, *6*, 1091–1104.

Wu, D. L. (2004), Mesoscale gravity wave variances from AMSU-A radiances, *Geophys. Res. Lett.*, *31*, L12114, doi:10.1029/2004GL019562.

Wu, D. L., and J. W. Waters (1996a), Gravity-wave-scale temperature fluctuations seen by the UARS MLS, *Geophys. Res. Lett.*, *23*(23), 3289–3292.

Wu, D. L., and J. W. Waters (1996b), Satellite observations of atmospheric variances: A possible indication of gravity waves, *Geophys. Res. Lett.*, *23*(24), 3631–3634.

Wu, D. L., and F. Zhang (2004), A study of mesoscale gravity waves over the North Atlantic with satellite observations and a mesoscale model, *J. Geophys. Res.*, *109*, D22104, doi:10.1029/2004JD005090.

M. J. Alexander, NWRA, Colorado Research Associates Division, 3380 Mitchell Lane, Boulder, CO 80301, USA. (alexand@cora.nwra.com)

J. Barnett and C. Hepplewhite, Clarendon Laboratory, Oxford University, Parks Road, Oxford, OX1 3PU, UK.

C. Cavanaugh, M. Coffey, C. Craig, T. Eden, G. Francis, C. Halvorson, J. Hannigan, R. Khosravi, D. Kinnison, S. Massie, and B. Nardi, NCAR, P.O. Box 3000, Boulder, CO 80307, USA.

V. Dean and J. Gille, Center for Limb Atmospheric Sounding, 216 UCB, University of Colorado, Boulder, CO 80309-0216, USA.

A. Lambert, Jet Propulsion Laboratory, California Institute of Technology, 4800 Oak Grove Drive, Pasadena, CA 91109, USA.